FINITE BLOCKLENGTH SYMMETRIC INFORMATION RATE OF SOQPSK

Cenk Sahin and Erik Perrins
Department of Electrical Engineering & Computer Science
University of Kansas
Lawrence, KS 66045
cenksahin@ittc.ku.edu

ABSTRACT

In this paper we compute a lower bound, namely the dependence testing (DT) bound, on the maximum achievable rates (expressed in bits/channel use) with military standard shaped-offset quadrature phase shift-keying (SOQPSK-MIL) and aeronautical telemetry SOQPSK (SOQPSK-TG) schemes over additive white Gaussian noise (AWGN) channels under finite code blocklength, probability block error and equiprobable input constraints. The DT bound results for SOQPSK-MIL and SOQPSK-TG are used to lower bound their respective spectral efficiencies (expressed in bits/s/Hz). We simulate a serially concatenated convolutional code (SCCC) using SOQPSK-MIL as the inner code, and show that it performs within 1.1 dB of the SOQPSK-MIL DT bound for various coding rates. The numerical results also demonstrate the performance loss compared to the channel capacity due to the finite blocklength constraint.

INTRODUCTION

Shaped-offset quadrature phase-shift keying (SOQPSK) is a type of widely used bandwidth-efficient continuous phase modulation (CPM) [1]. The widespread use of SOQPSK is due to its constant signal envelope, which makes it robust against the distortion introduced by non-linear power amplifiers. As a result, SOQPSK can be used in low-cost, high-power miniature transmitters since non-linear amplifiers are compact, inexpensive, and highly efficient in converting limited (i.e. battery) power into radiated power. The constant envelope of CPM, and hence SOQPSK, signals comes with the price of mathematical intractability due to the memory in CPM signals. Consequently, recent work on the theoretical performance limits of CPM has resorted to simulation-based methods. In [2] a simulation-based technique to compute the capacity of channels with memory (i.e. CPM) was proposed. In [3] a similar method was used to compute the capacity of CPM while in [4] the best spectrally-efficient CPM modulations were investigated. In [5] we evaluated the capacities of two standardized versions of SOQPSK: military-standard SOQPSK (SOQPSK-MIL) [6] and aeronautical telemetry SOQPSK (SOQPSK-TG) [7].

The channel capacity is an important performance measure for communication systems operating without code blocklength constraints. However, in practical communication systems, due to delay requirements and memory limitations it is prohibitive to use asymptotically long codes. In addition, the use of finite blocklength codes results in a rate penalty—compared to the channel capacity—that strongly depends on the probability of error. The study of channel coding bounds in the finite blocklength regime has gained significant momentum after the seminal work of Polyanskiy et al. [8]. The authors developed new bounds on the maximum achievable rate for a given blocklength and a probability of block error [8]. In [9]

we introduced a simulation-based method to compute a lower bound called the dependence testing (DT) bound [8] on the maximum achievable coding rate with CPM over additive white Gaussian noise (AWGN) channels under finite blocklength, probability of error, and equiprobable input distribution constraints. The method in [9] uses a posteriori (AP) state transition probabilities of the trellis that models the CPM modulation, which are computed by the BCJR [10] algorithm.

In this paper, we apply the method developed in [9] to SOQPSK and evaluate the DT bound on the maximum achievable rates of SOQPSK-MIL and SOQPSK-TG over AWGN channels under an equiprobable input constraint. The DT bound is then used to lower bound the (maximum achievable) spectral efficiencies of SOQPSK-MIL and SOQPSK-TG under finite blocklength and probability of error constraints. SOQPSK-TG and SOQPSK-MIL differ in their frequency pulses and SOQPSK-TG achieves a superior spectral containment than SOQPSK-MIL due to its partial response. Optimal detection based on the CPM representation [11] requires a 512-state trellis for SOQPSK-TG while it requires only a 4-state trellis for SOQPSK-MIL. However; reduced-complexity detection methods such as pulse amplitude modulation (PAM) [12, 13] and pulse truncation (PT) [14, 15] exist and result in 4-state detectors for SOQPSK-TG that perform within 0.1 dB of the optimal detector. The evaluation of the DT bound for SOQPSK-MIL and SOQPSK-TG establishes a yardstick by which practical systems can be judged and allows a performance comparison of the two types of SOQPSK. Because a fair performance comparison between two versions of SOQPSK would require them to have the same detection complexity, we implement a PAM-based suboptimal detector for SOQPSK-TG.

This paper is organized as follows. First, we describe the signal model for SOQPSK, including the 4-state transmitter model and the PAM approximation of SOQPSK. Next, we describe the computation of the DT bound and the resulting bound on the spectral efficiency of SOQPSK. Last, we present numerical results with SOQPSK-MIL and PAM-based SOQPSK and state our conclusions.

SOQPSK SIGNAL MODEL

The complex baseband SOQPSK signal can be represented as a CPM signal [1] of the form

$$s(t;\boldsymbol{\alpha}) \triangleq \sqrt{\frac{E_s}{T_s}} \exp\left\{j\psi(t;\boldsymbol{\alpha})\right\} \tag{1}$$

where $\boldsymbol{\alpha} \triangleq \{\alpha_i\}$ is the transmitted symbol sequence drawn from a *ternary* alphabet, i.e. $\alpha_i \in \{-1, 0, +1\}$, T_s is the *symbol interval* and E_s is the *energy per symbol*. The phase of the signal, denoted by $\psi(t;\boldsymbol{\alpha})$, is of the form

$$\psi(t;\boldsymbol{\alpha}) \triangleq 2\pi h \sum_i \alpha_i q(t - iT_s) \tag{2}$$

where $i \in \mathbb{Z}$ is the discrete-time index and $h = 1/2$ is the *modulation index*. The *phase response* $q(t)$ is defined as the time integral of the *frequency pulse* $g(t)$. The frequency pulse $g(t)$ has a duration of LT_s where $L \in \mathbb{Z}^+$, and the area under $g(t)$ is $1/2$. When $L = 1$, the signal is said to be *full-response* and when $L > 1$ it is *partial-response*. For $nT_s \le t < (n+1)T_s$ the signal phase given in (2) may be expressed as

$$\psi(t;\boldsymbol{\alpha}) = \underbrace{2\pi h \sum_{i=n-L+1}^{n} \alpha_i q(t - iT_s)}_{\theta(t)} + \underbrace{\pi h \sum_{i=0}^{n-L} \alpha_i}_{\theta_{n-L}}, \tag{3}$$

where the *phase state* θ_{n-L} is drawn from an alphabet of 4 values, $\theta_{n-L} \in \{0, \pi/2, \pi, 3\pi/2\}$, when taken modulo 2π.

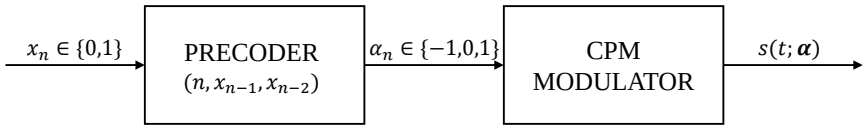

Figure 1: Transmitter model for SOQPSK.

With SOQPSK, unlike CPM, the symbol sequence transmitted over the channel $\boldsymbol{\alpha}$ is not the underlying bit sequence $\boldsymbol{x} \triangleq \{x_i\},\ x_i \in \{-1, +1\}$. The ternary symbol sequence $\boldsymbol{\alpha}$ is derived from the original bit sequence $\boldsymbol{x}$ by the precoding operation defined by the rule [16]

$$\alpha_n(\boldsymbol{x}) = (-1)^{n+1}(2x_{n-1} - 1)(x_n - x_{n-2}) \tag{4}$$

as shown in Fig. 1 [11]. The precoder orients the phase of the CPM signal so that it behaves like the phase of an offset-QPSK (OQPSK) signal driven by the symbol sequence $\boldsymbol{x}$. As a result of precoding, in any given symbol interval, α_i is drawn from one of the two *binary* alphabets: $\{-1, 0\}$ or $\{0, +1\}$ [16]. Consequently, SOQPSK can be viewed as a *constrained* ternary CPM. There are two standardized versions of SOQPSK, namely military standard SOQPSK (SOQPSK-MIL) [6] and aeronautical telemetry SOQPSK (SOQPSK-TG). SOQPSK-MIL uses a full-response ($L = 1$) rectangular frequency pulse while SOQPSK-TG uses a longer ($L = 8$) and smoother frequency pulse (defined in [7]) that results in superior spectral containment [17, Fig. 3], but also higher *optimal* detection complexity.

SOQPSK TRELLIS

In (4) we see that α_n is a function of three binary-valued state variables x_{n-1}, x_{n-2} and n-even/n-odd which leads to an 8-state trellis to describe the precoder in Fig. 1[18]. We follow the approach taken in [17] that handles the state variable n-even/n-odd by a time-varying two-section trellis shown in Fig. 2. The state variables $x_{n-1}$and x_{n-2} are ordered in such a way that the *in-phase* (I) bit is always the most significant and the *quadrature* (Q) bit is always the least significant. The labels above each branch are the input-bit/output-symbol pair x_n/α_n for the system in Fig. 1. The *one-to-one mapping* between the phase states of the CPM modulator $\theta_{n-L} \in \{0, \pi/2, \pi, 3\pi/2\}$ and the precoder trellis states $S_n \in \{00, 01, 10, 11\}$ [11, Fig. 4] paves the way for reduced complexity detection algorithms operating on the 4-state trellis shown in Fig. 2.

SOQPSK DETECTION

The optimal maximum likelihood sequence detection (MLSD) of SOQPSK requires a trellis. Trellis-based SOQPSK detectors were first studied in [18]. Because SOQPSK-MIL is full-response, the trellis described in the previous section can be used for its optimal detection. However, an optimal detector for SOQPSK-TG requires a 512-state trellis, which makes the optimal detection unfeasible. As previously shown in [17], a *pulse amplitude modulation* (PAM) approximation of CPM [12, 13] allows the 4-state full response trellis shown in Fig. 2 to be used for *near-optimal* detection of SOQPSK-TG. Below we briefly summarize this approach.

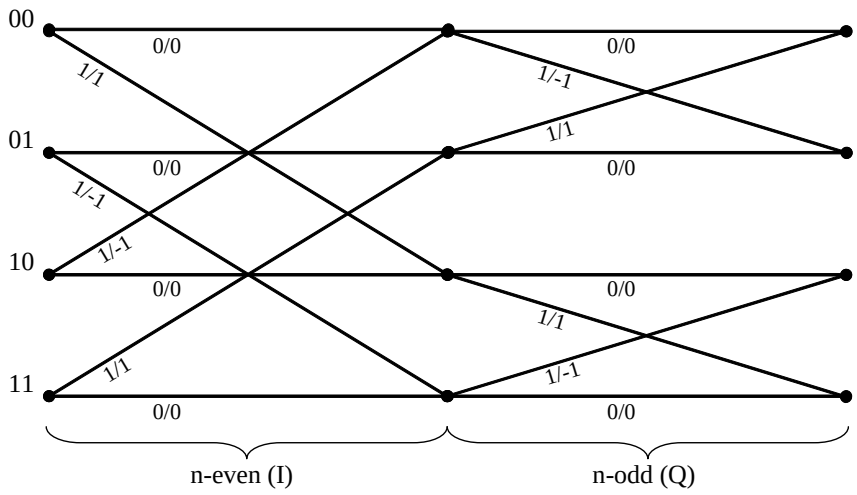

Figure 2: The 4-state time-varying trellis for the precoder. The states are labeled with the state vector S_n and the branches are labeled with the input-bit/output-symbol pair x_n/α_n.

With the PAM decomposition approach, a CPM signal can be expressed as a sum of K amplitude modulated pulses in the form

$$s(t;\boldsymbol{\alpha}) = \sqrt{\frac{E_s}{T_s}} \sum_{k=0}^{K-1} \sum_{i} \beta_{k,i} g_k(t - iT_s). \tag{5}$$

The full definitions that describe the pulses $\{g_k(t)\}$ and pseudo-symbols $\{\beta_{k,i}\}$ for SOQPSK can be found in [13]. The energy of the signal $s(t;\boldsymbol{\alpha})$ is mostly concentrated in the first two pulses in the sum (5), called the *principal pulses* in [19]. An approximation based on the principal pulses given as

$$s(t;\boldsymbol{\alpha}) \approx \sqrt{\frac{E_s}{T_s}} \sum_{k=0}^{1} \sum_{i} \beta_{k,i} g_k(t - iT_s) \tag{6}$$

results in a 4-state SOQPSK-TG detector that performs within 0.1 dB of the optimal detector.

FINITE BLOCKLENGTH SYMMETRIC INFORMATION RATE OF SOQPSK

In this section we describe a simulation-based method to compute a lower/achievability bound on the maximum achievable rate with SOQPSK schemes over AWGN channels under finite blocklength and probability of block error constraints. This method is the specialization of the method described in [9] for general CPM schemes. We consider the communication system shown in Fig. 3. A channel encoder denoted by f maps one of N equiprobable messages to a length-n sequence of binary symbols, i.e. $f : \{1, \cdots, N\} \to \{0,1\}^n$. The code size N satisfies $\log_2 N = k \in \mathbb{Z}^+$; accordingly, we denote the encoder input by $U_1^k = U_1 \cdots U_k$ where $u_j \in \{0,1\}$. In this paper, we denote random variables by upper-case symbols, and arbitrary realizations of random variables by lower-case symbols. The encoder output is denoted by the sequence $X_1^n = X_1 \cdots X_n$ where $x_i \in \{0,1\}$.

The symbol sequence X_1^n is modulated as a SOQPSK signal denoted by $s\left(t; X_1^n\right)$, and transmitted over an additive white Gaussian noise (AWGN) channel resulting in the received signal

$$r\left(t; X_1^n\right) = s\left(t; X_1^n\right) + w(t) \tag{7}$$

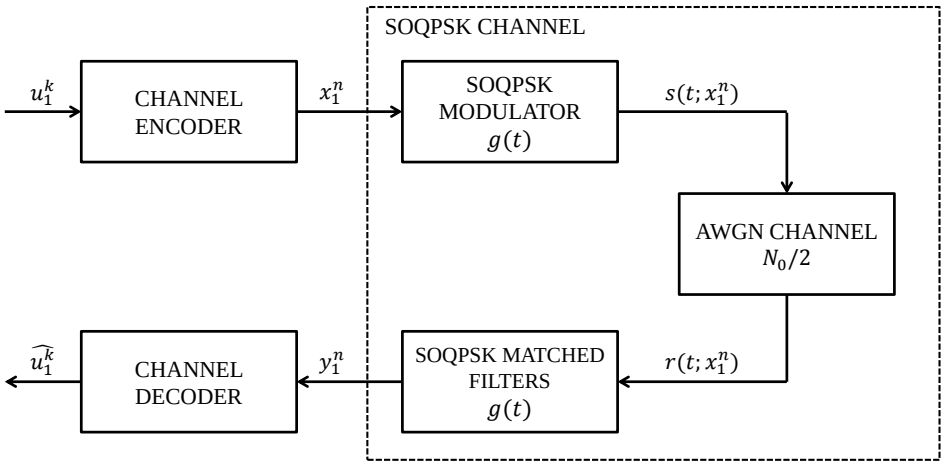

Figure 3: The block diagram of a communication system over an AWGN channel with a SOQPSK scheme and a finite blocklength channel code.

where $w(t)$ is Gaussian noise with a two-sided power spectral density $N_0/2$. The received waveform $r\left(t; X_1^n\right)$ is sampled into the sequence Y_1^n, which is a sufficient statistic for decoding purposes.[1] At the receiver a decoder operating on Y_1^n outputs an estimate of the transmitted message (information bit sequence) denoted by $\widehat{U_1^k}$. The probability of block error is given by $\Pr\{\widehat{U_1^k} \neq U_1^k\}$. To summarize, we model an AWGN channel with a SOQPSK scheme as a SOQPSK channel with input X_1^n, and output Y_1^n as shown in Fig. 3, where the input-output relationship is governed by the SOQPSK modulator and the additive Gaussian noise. The SOQPSK channel coding rate is given by $R = \frac{\log_2 N}{n}$ bits/channel use.

According to the dependence testing (DT) bound [8], given a discrete-input continuous-output channel $p_{Y_1^n|X_1^n}$, for an arbitrary input distribution $P_{X_1^n}$, there *exists* a code with N codewords, whose average probability of error denoted by $\epsilon(n, N)$, satisfies

$$\epsilon(n, N) \leq \mathbb{E}\left[\exp\left\{-\left[i\left(X_1^n, Y_1^n\right) - \log\frac{N-1}{2}\right]^+\right\}\right] \tag{8}$$

where $[a]^+ = a$ if $a \geq 0$, and $[a]^+ = 0$ otherwise; $i\left(X_1^n, Y_1^n\right)$ is defined by

$$i\left(X_1^n, Y_1^n\right) \triangleq \log\frac{p_{Y_1^n|X_1^n}\left(Y_1^n|X_1^n\right)}{p_{Y_1^n}\left(Y_1^n\right)}; \tag{9}$$

$\exp\{\cdot\}$ and $\log$ have the same base, and the expected value is taken according to the joint distribution $p_{Y_1^n|X_1^n}P_{X_1^n}$. We will denote the right hand side of (8) by $\epsilon_{\mathrm{DT}}(n, N)$. To convert the upper bound on the probability of error $\epsilon(n, N) \leq \epsilon_{\mathrm{DT}}(n, N)$ to a lower bound on the maximum achievable code size for a given probability of error constraint ϵ, we find the largest N such that $\epsilon_{\mathrm{DT}}(n, N) \leq \epsilon$ [8]. Accordingly—from the DT bound—there *exists* a code with blocklength n and average probability of error ϵ, whose size denoted by $N(n, \epsilon)$ satisfies

$$N(n, \epsilon) \geq \max\{N : \epsilon_{\mathrm{DT}}(n, N) \leq \epsilon\} \tag{10}$$

[1]Here Y_i may be a vector of samples; as long as Y_1^n is a sufficient statistic for $r\left(t; X_1^n\right)$ the sampling rate or the sampling method is irrelevant.

where we will denote the right hand side by $N_{\mathrm{DT}}(n,\epsilon)$, i.e. $N(n,\epsilon) \geq N_{\mathrm{DT}}(n,\epsilon)$. Then we get an achievability bound on the coding rate by $R(n,\epsilon) \geq R_{\mathrm{DT}}(n,\epsilon)$ where $R_{\mathrm{DT}}(n,\epsilon) = \log_2 N_{\mathrm{DT}}(n,\epsilon)/n$. Due to the memory of SOQPSK waveforms neither $p_{Y_1^n|X_1^n}$ nor $p_{Y_1^n}$ is analytically tractable. Accordingly, $\epsilon_{\mathrm{DT}}(n,N)$ is computed by simulations for the SOQPSK channel.

We choose the input distribution $P_{X_1^n}$ as equiprobable, i.e. $P_{X_1^n}(x_1^n) = 2^{-n}$ for all x_1^n. Accordingly, our information-theoretic results are under an equiprobable input distribution constraint, and we refer to the maximum achievable rate as the maximum achievable symmetric information rate [20]. Then $i\left(X_1^n, Y_1^n\right)$ (with base 2) can be written as

$$i\left(X_1^n, Y_1^n\right) = n + \log_2 P_{X_1^n|Y_1^n}\left(X_1^n|Y_1^n\right). \tag{11}$$

Furthermore, we can write $\log_2 P_{X_1^n|Y_1^n}\left(X_1^n|Y_1^n\right)$ as a sum of (dependent) random variables by

$$\log_2 P_{X_1^n|Y_1^n}\left(X_1^n|Y_1^n\right) = \sum_{i=1}^{n} \log_2 P(X_i|S_{i-1}(X_1^{i-1})Y_1^n) \tag{12}$$

where $S_{i-1}(X_1^{i-1})$ is the state of the trellis modeling the SOQPSK modulator at the beginning of the symbol interval *i* uniquely determined by X_1^{i-1}, and $S_{i-1}(X_1^{i-1}) \in \mathcal{S}$ where $\mathcal{S}$ is the state space of the particular SOQPSK trellis. When replacing X_1^{i-1} by $S_{i-1}(X_1^{i-1})$ we used the fact that the memory of the CPM modulator at the beginning of the symbol interval *i*—due to $X_1 \cdots X_{i-1}$—is summarized in the value of the trellis state $S_{i-1}(X_1^{i-1})$. Consequently, we write the DT bound in (8) for SOQPSK by

$$\epsilon(n,N) \leq \mathbb{E}\left[\exp\left\{-\left[\sum_{i=1}^{n} \log_2 P(X_i|S_{i-1}(X_1^{i-1})Y_1^n) - \log_2 \frac{N-1}{2^{n+1}}\right]^+\right\}\right] \tag{13}$$

where $\exp\{\cdot\}$ is base 2.

Since the communication system under consideration is ergodic, we can compute the expected value in (13) with time averages via Monte Carlo simulations as described below. The BCJR algorithm [10] is a suitable tool for this task with its ability to compute the a posteriori probabilities (APPs) of all state transitions on the SOQPSK trellis for all symbol intervals denoted by $P(S_i, S_{i-1}|Y_1^n), 1 \leq i \leq n$, where $S_i, S_{i-1} \in \mathcal{S}$, and we assume that the SOQPSK modulator starts at a known state $S_0 = s_0$. We note the equivalence:

$$P(X_i|S_{i-1}(X_1^{i-1})Y_1^n) = P(S_i(X_1^i)|S_{i-1}(X_1^{i-1})Y_1^n). \tag{14}$$

Then $P(X_i|S_{i-1}(X_1^{i-1})Y_1^n)$—the APP that conditioned on being in state $S_{i-1}(X_1^{i-1})$ the state transition associated with symbol X_i occurs—is given by the expression

$$P(X_i|S_{i-1}(X_1^{i-1})Y_1^n) = \frac{P(S_i(X_1^i)S_{i-1}(X_1^{i-1})|Y_1^n)}{P(S_i(X_1^i)S_{i-1}(X_1^{i-1})|Y_1^n) + P(S_i(X_1^{i-1}X_i')S_{i-1}(X_1^{i-1})|Y_1^n)} \tag{15}$$

where X_i' denotes the binary complement of X_i. In other words, $S_i(X_1^{i-1}X_i')$ is "the other state" (other than $S_i(X_1^i)$) that is connected to $S_{i-1}(X_1^{i-1})$ in the SOQPSK trellis.

For the computation of the DT bound for a given SOQPSK scheme and a given SNR value, we generate length-n blocks of binary input sequences. Each input sequence x_1^n is modulated as a SOQPSK signal $s(t;x_1^n)$ and an AWGN sequence is added to $s(t;x_1^n)$ according to the SNR value E_s/N_0. Then the samples of the output signal $r(t;x_1^n)$ denoted by y_1^n—that form a sufficient statistic for decoding purposes—are fed into the BCJR algorithm. The trellis state sequence corresponding to x_1^n is given by $s_0^n(x_1^n)$. Note that

both are known quantities. The BCJR algorithm is used to compute $P(s_i s_{i-1}|y_1^n)$ for all $s_i, s_{i-1} \in \mathcal{S}$ and $1 \leq i \leq n$. Finally, $P(x_i|s_{i-1}(x_1^{i-1})y_1^n)$ is computed from (15) for all $1 \leq i \leq n$, which are then used to compute $\log_2 P_{X_1^n|Y_1^n}(x_1^n|y_1^n)$. Because the quantity $\log_2 P_{X_1^n|Y_1^n}(x_1^n|y_1^n)$ only depends on the particular SOQPSK scheme and the SNR value, and does not depend on the code size N, we can use $\log_2 P_{X_1^n|Y_1^n}(x_1^n|y_1^n)$ to get simulation points for a set of N values by the expression inside the expected value in (13). In other words, a single Monte Carlo simulation can be used to compute $\epsilon_{\mathrm{DT}}(n, N)$ for a set of N values. Once a sufficiently large number of blocks have been simulated, from the set of values of $\epsilon_{\mathrm{DT}}(n, N)$ we determine $N_{\mathrm{DT}}(n, \epsilon)$, and $R_{\mathrm{DT}}(n, \epsilon)$ for a given probability of error constraint ϵ from (10). After computing $R_{\mathrm{DT}}(n, \epsilon)$ for a given value of E_s/N_0, we compute the *energy per information bit*, E_b, by replacing the *code rate*, R by $R_{\mathrm{DT}}(n, \epsilon)$, in the well-known relationship $E_s = RE_b$.

The method described above can be used for reduced-complexity SOQPSK detection methods such as pulse amplitude modulation (PAM) [11, 12, 13] and pulse truncation (PT) [14, 15]. In that case the BCJR algorithm operates on the sequence y_1^n generated by the particular reduced complexity detector, and the reduced-complexity SOQPSK trellis, resulting in a maximum achievable rate lower bound constrained on the particular reduced-complexity detection method.

FINITE BLOCKLENGTH SPECTRAL EFFICIENCY OF SOQPSK

In practical communication systems, a performance measure related to—but more important than—the communication rate is the spectral efficiency (expressed in bits/s/Hz), which takes into account the spectral representation of the modulated waveform. Coding rate alone can be misleading. For example, despite having nearly equal symmetric information rates (under no blocklength constraints), SOQPSK-TG spectral efficiency is significantly higher than that of SOQPSK-MIL [5]. To compute the spectral efficiency of SOQPSK under a finite blocklength contraint, we first define the normalized symbol rate for a given SOQPSK scheme denoted by R_s (channel use/s/Hz) as the symbol rate when only 1 Hz of bandwidth is available as in [4]. We note that R_s depends heavily on the particular SOQPSK scheme under consideration. In the computation of R_s we define the bandwidth as the one that contains 99.9% of the signal power. Then the (maximum achievable) spectral efficiency of SOQPSK under a finite blocklength, and a probability of error constraint can be lower bounded by the product of R_s and the lower bound on the maximum achievable rate computed by the DT bound denoted by $R_{\mathrm{DT}}(n, \epsilon)$.

NUMERICAL RESULTS

For the numerical results we compute the DT bound on the maximum achievable rate for SOQPSK-MIL, and for SOQPSK-TG with a PAM-based detector (SOQPSK-TG-PAM). Note that both SOQPSK-MIL and SOQPSK-TG-PAM have the same detection complexity (i.e. 4-state trellis), which allows a fair comparison. The probability of block error constraint is $\epsilon = 10^{-3}$. We set the number of information bits to $\log_2 N = 2048$. For each scheme, for coding rates of $R = \frac{1}{2}, \frac{2}{3}$ and $\frac{4}{5}$ (code blocklength values of $n = 4196, 3072$, and 2560 respectively) we compute the minimum required SNR per information bit value $\frac{E_b}{N_0}$ such that the right hand side of the DT bound in (13) denoted by $\epsilon_{\mathrm{DT}}(2048/R, 2^{2048})$ for the given values of n and N, is less than the probability of error constraint 10^{-3}. As a result, for each modulation scheme we get three DT bound points. For reference, we also compute the symmetric information rate for each modulation (i.e. capacity under equiprobable distribution) by simulation via the method described in [3]. All four quantities are shown in Fig. 5 as a function of $\frac{E_b}{N_0}$, where the vertical axis represents the spectral efficiency (bits/s/Hz); accordingly, all quantities are scaled by respective normalized symbol rates

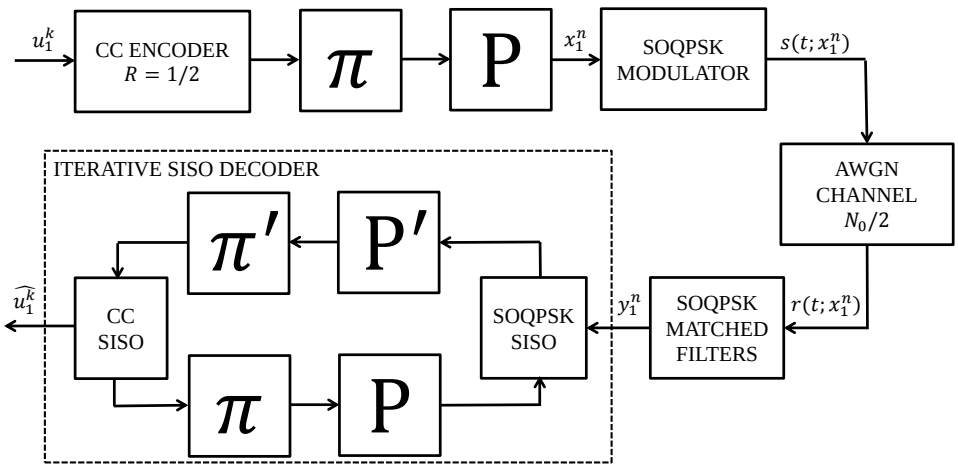

Figure 4: The block diagram of a punctured SCCC scheme with a rate $\frac{1}{2}$ convolutional code as the outer code, and the SOQPSK-MIL modulator as the inner code.

R_s. The normalized symbol rate R_s of SOQPSK-TG is 1.00 while it is 0.56 for SOQPSK-MIL for the bandwidth containing 99.9% of the signal power. We observe in Fig. 5 that the gap between the channel capacity curves and the DT bound points is approximately 0.6 dB with both modulation schemes. This gap will increase as the probability of error constraint or the number of information bits decreases.

In addition, we implement a serially concatenated convolutional coding (SCCC) [21] scheme over the AWGN channel with SOQPSK-MIL. The SCCC scheme consists of an outer $(5, 7)$ convolutional encoder of rate $\frac{1}{2}$, and SOQPSK-MIL as the inner code. In addition, rates of $\frac{2}{3}$ and $\frac{4}{5}$ are achieved by puncturing the outer encoder output according to the puncturing schemes described in [22]. The SCCC scheme block diagram is shown in Fig. 4. The block labeled with π (π') represents the interleaver (deinterleaver), while the block P (P') represents the puncturing (depuncturing) operation. An iterative *soft-input soft-output* (SISO [23]) decoder—carrying out iterations between the convolutional code SISO (CC SISO) module and the SOQPSK-MIL SISO module—is used at the receiver. As with the DT bound the number of information bits is set to 2048 (bits) while the target probability of error is $\epsilon = 10^{-3}$. For each SCCC rate we determine the minumum required SNR such that $\epsilon_{\mathrm{SCCC}} \leq 10^{-3}$, where ϵ_{SCCC} is the probability of block error computed by simulations. We observe in Fig. 4 that the SCCC scheme performs approximately within 1.1 dB of the DT bound.

CONCLUSIONS

Shaped-offset quadrature phase-shift keying (SOQPSK) is a type of widely used bandwidth-efficient continuous phase modulation (CPM), standardized for military applications (SOQPSK-MIL) and aeronautical telemetry (SOQPSK-TG). As practical communication systems are bound to operate with finite block-length codes (due to delay and memory constraints), it becomes increasingly important to investigate the finite blocklength coding performance of SOQPSK schemes. In this paper, we used a simulation-based method to compute lower bounds on the maximum achievable rate (achievability bounds) with SOQPSK-MIL and SOQPSK-TG modulations, over additive white Gaussian noise (AWGN) channels under finite code blocklength, probability block error and equiprobable input distribution constraints. Each achievability bound establishes a yardstick by which practical practical SOQPSK schemes can be judged. We

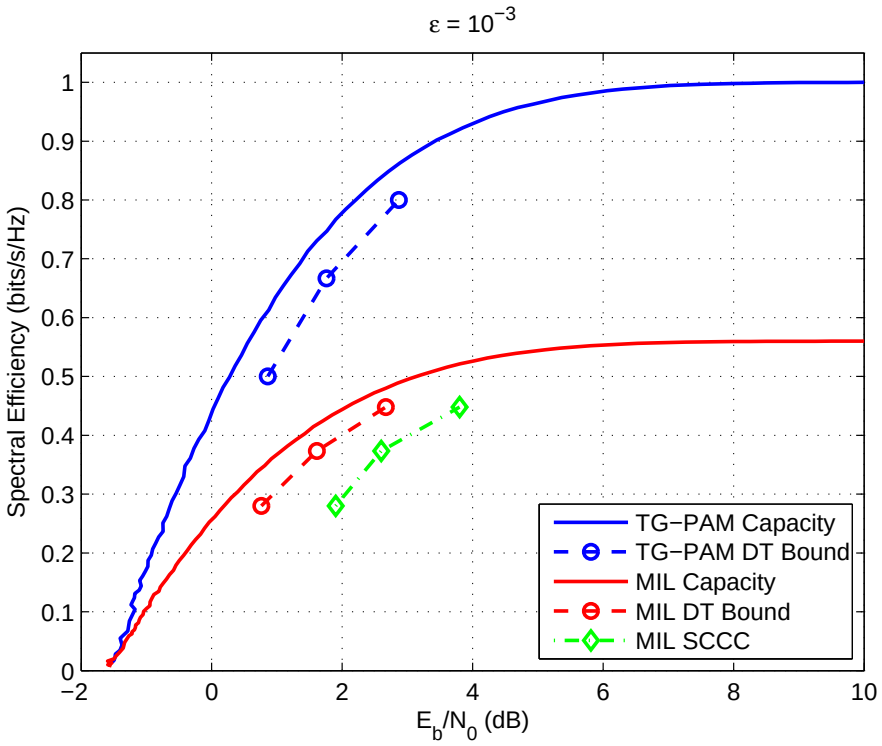

Figure 5: The spectral efficiency, and the DT lower bound on the spectral efficiency for SOQPSK-MIL and SOQPSK-TG-PAM, along with the performance of a SCCC using SOQPSK-MIL as the inner code for rates $\frac{1}{2}$, $\frac{2}{3}$ and $\frac{4}{5}$. The probability of block error contraint for the DT bound is $\epsilon = 10^{-3}$.

simulated a serially concatenated convolutional code (SCCC) using SOQPSK-MIL as the inner code, which performed within 1.1 dB of the SOQPSK-MIL achievability bound for various coding rates.

REFERENCES

[1] J. B. Anderson, T. Aulin, and C.-E. Sundberg, *Digital Phase Modulation*. New York: Plenum Press, 1986.

[2] D. Arnold, H.-A. Loeliger, P. Vontobel, A. Kavcic, and W. Zeng, "Simulation-based computation of information rates for channels with memory," *IEEE Trans. Inform. Theory*, vol. 52, pp. 3498–3508, Aug. 2006.

[3] K. Padmanabhan, S. Ranganathan, S. P. Sundaravaradhan, and O. M. Collins, "General CPM and its capacity," in *Proc. Int. Symp. Inf. Theory*, (Adelaide, Australia), pp. 750–754, Sep. 2005.

[4] A. Perotti, A. Tarable, S. Benedetto, and G. Montorsi, "Capacity-achieving CPM schemes," *IEEE Trans. Inf. Theory*, vol. 56, pp. 1521–1541, Apr. 2010.

[5] C. Sahin and E. Perrins, "The capacity of SOQPSK-TG," in *Proc. of the 2011 IEEE Military Commun. Conf.*, (Baltimore, MD), pp. 555–560, Nov. 2011.

[6] D. I. S. Agency, "Department of Defense interface standard, interoperability standard for single-access 5-kHz and 25-kHz UHF satellite communications channels." Tech. Rep. MIL-STD-188-181B, Department of Defense, Mar. 1999.

[7] Range Commanders Council Telemetry Group, Range Commanders Council, White Sands Missile Range, New Mexico, *IRIG Standard 106-04: Telemetry Standards*, 2004. (Available on-line at http://www.ntia.doc.gov/osmhome/106.pdf).

[8] Y. Polyanskiy, H. Poor, and S. Verdu, "Channel coding rate in the finite blocklength regime," *IEEE Trans. Inf. Theory*, vol. 56, pp. 2307 –2359, May 2010.

[9] C. Sahin and E. Perrins, "On the symmetric information rate of CPM in the finite blocklength region," in *Proc. of the 2015 IEEE Military Commun. Conf.*, (Tampa Bay, FL), pp. 815–819, Oct. 2015.

[10] L. Bahl, J. Cocke, F. Jelinek, and J. Raviv, "Optimal decoding of linear codes for minimizing symbol error rate," *IEEE Trans. Inform. Theory*, vol. 20, pp. 284–287, Mar. 1974.

[11] E. Perrins and M. Rice, "Reduced-complexity approach to iterative detection of SOQPSK," *IEEE Trans. Commun.*, vol. 55, pp. 1354–1362, Jul. 2007.

[12] P. A. Laurent, "Exact and approximate construction of digital phase modulations by superposition of amplitude modulated pulses (AMP)," *IEEE Trans. Commun.*, vol. 34, pp. 150–160, Feb. 1986.

[13] E. Perrins and M. Rice, "PAM representation of ternary CPM," *IEEE Trans. Commun.*, vol. 56, pp. 2020–2024, Dec. 2008.

[14] T. Aulin, C.-E. Sundberg, and A. Svensson, "Viterbi detectors with reduced complexity for partial response continuous phase modulation," in *Proc. National Telecommun. Conf., NTC'81*, (New Orleans, LA), pp. A7.6.1–A7.6.7, Nov./Dec. 1981.

[15] A. Svensson, C.-E. Sundberg, and T. Aulin, "A class of reduced-complexity Viterbi detectors for partial response continuous phase modulation," *IEEE Trans. Commun.*, vol. 32, pp. 1079–1087, Oct. 1984.

[16] M. Simon, *Bandwidth-Efficient Digital Modulation With Application to Deep-Space Communication*. New York: Wiley, 2003.

[17] E. Perrins and M. Rice, "Simple detectors for shaped-offset QPSK using the PAM decomposition," in *Proc. IEEE Global Telecommun. Conf.*, (St. Louis, MO), pp. 408–412, Nov./Dec. 2005.

[18] L. Li and M. Simon, "Performance of coded OQPSK and MIL-STD SOQPSK with iterative decoding," *IEEE Trans. Commun.*, vol. 52, pp. 1890–1900, Nov. 2004.

[19] U. Mengali and M. Morelli, "Decomposition of M-ary CPM signals into PAM waveforms," *IEEE Trans. Inform. Theory*, vol. 41, pp. 1265–1275, Sep. 1995.

[20] H. D. Pfister, J. B. Soriaga, and P. H. Siegel, "On the achievable information rates of finite state ISI channels," in *Proc. IEEE Global Telecommun. Conf.*, vol. 5, (San Antonio, TX), pp. 2992–2996, Nov. 2001.

[21] S. Benedetto, D. Divsalar, G. Montorsi, and F. Pollara, "Serial concatenation of interleaved codes: Performance analysis, design, and iterative decoding," *IEEE Trans. Inform. Theory*, vol. 44, pp. 909–926, May 1998.

[22] Y. Yasuda, K. Kashiki, and Y. Hirata, "High-rate punctured convolutional codes for soft decision Viterbi decoding," *IEEE Trans. Commun.*, vol. 32, pp. 315–319, Mar. 1984.

[23] S. Benedetto, D. Divsalar, G. Montorsi, and F. Pollara, "A soft-input soft-output APP module for iterative decoding of concatenated codes," *IEEE Commun. Lett.*, vol. 1, pp. 22–24, Jan. 1997.